E\PCOS 2013

Tunable nanophotonic circuits based on phase-change materials

Carlos Rios[1], Peiman Hosseini[2], C. David Wright[3], Harish Bhaskaran[2] and Wolfram H P Pernice[1]

[1]Karlsruhe Institut für Technologie, D-76344 Eggenstein-Leopoldshafen, Germany
[2]Department of Materials, University of Oxford, Oxford OX1 3PH, UK
[3]College of Engineering, Mathematics & Physical Sciences, University of Exeter, Exeter, UK

ABSTRACT

We present preliminary results of the characterization of the optical response of $Ge_2Sb_2Te_5$ (GST) thin-films integrated with Si_3N_4 nanophotonic circuits at telecom wavelengths. Transmission measurements are carried out GST thin-films of varying width deposited on top of ring resonators. The nanophotonics circuits are fabricated and optimized in order to find the best response when GST is placed atop the waveguiding layer. Our results for the absorption/transmission properties at different phase states of GST thin-films paves the way towards a all-photonic non-volatile memories.

Key words: nanophotonic circuits, phase-change memories, optical resonator.

1. INTRODUCTION

The properties of phase change materials capable of switching from the amorphous to crystalline state in a matter of picoseconds [1-3], and the ability to retain such states for very long periods of time [4,5] have created significant interest in the recent years. $Ge_2Sb_2Te_5$ (GST) is a common phase change material, and its use in phase change memories (PCMs) has been a subject of intense research. PCMs promise to bridge the gap between fast switching but short term on-chip memories and long-term but slow storage systems such as solid-state systems and hard-drives [4, 6,7].

The demonstrated scalability of GST down to 6nm thin films [5,8] and the strong contrast between the optical properties of this material in the amorphous and crystalline state [9], together with Si-based devices could allow the creation of fully functional photonic non-volatile memories [10]. In particular, silicon nitride-on-insulator is emerging as a promising material platform to fabricate such nanophotonic components because of its broad band transparency window, covering telecom and visible wavelengths [11,12].

In this work, we present a fabrication process for photonic circuits based on the architecture proposed in [10], which compromises a microring resonator as substrate for the GST layer coupled to a nanophotonic waveguide. We present preliminary experimental results of the characterization for devices employing the amorphous state of the phase change material and simulation results of the actual geometry used in the process.

2. SIMULATIONS

The modal profiles of the GST covered waveguide cross-section illustrated in **Fig. 1a** are calculated using a Finite Element Method (FEM)**.** Our device consists of a waveguide covered with a 10nm GST layer. A second 10nm thick layer of indium tin oxide (ITO) is also included as needed for capping the GST after the deposition process in order to avoid oxidation. The rectangular waveguide is designed to be half-etched into a 330nm silicon nitride-on-insulator substrate.

During the simulations the width and the wavelength were swept in order to find optimal parameters, where the contrast between absorption coefficient α in the amorphous and the crystalline states of GST were significantly high, and, at the same time, where the waveguide supports only monomode operation. The results in **Fig. 1d** suggest that the waveguide width does not have a strong effect on the contrast between the two states for a wavelength λ=1.57 µm. Nevertheless, we have found that for a width larger than 1.4µm a second order mode can be exited for reasonable transmission. Therefore, we have fixed our waveguide width to 1.3µm and calculated the wavelength dependence in the range were the experimental measurements were carried out; the results are illustrated in **Fig. 1e.**
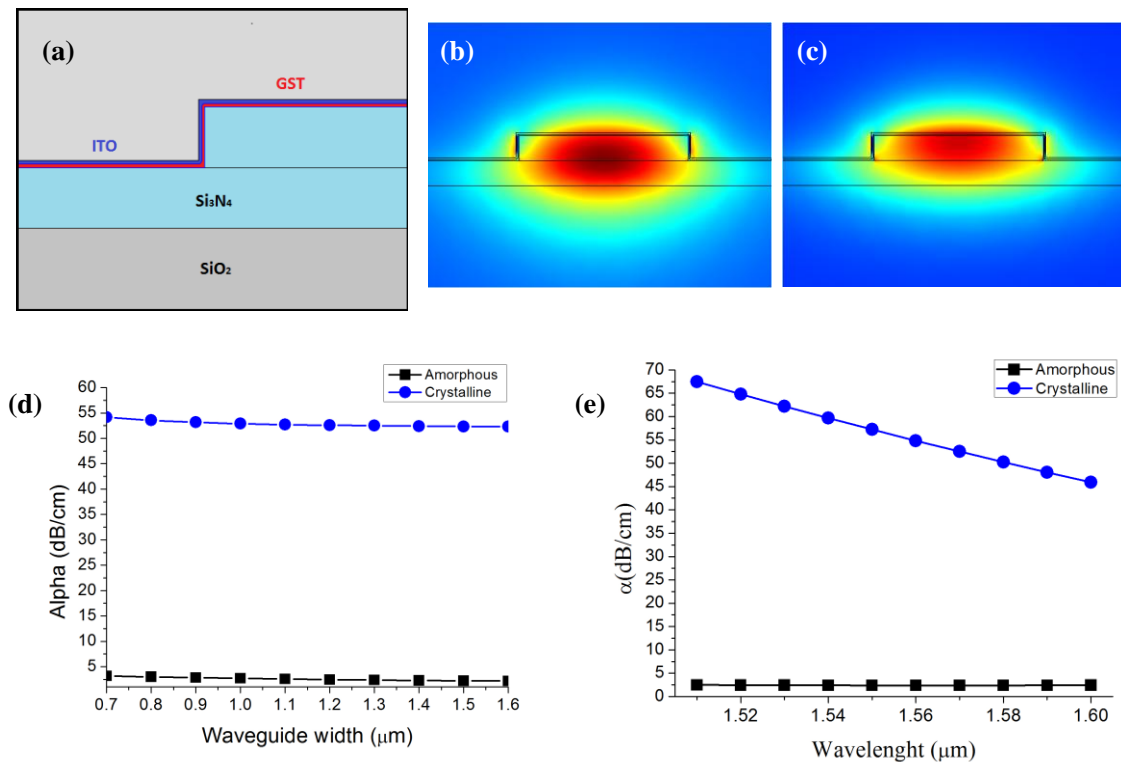
Fig. 1: (a)Waveguide geometry and materials used in the FEM simulation. (b) Calculated TE_o modal profile when the GST is in the amorphous state and (c) when it is in the crystalline state. (d) Absorption coefficient against width of the waveguide for a wavelength of λ=1.57µm. (e) Absorption coefficient dependence on the wavelength for a width of 1.3 µm.

3. FABRICATION

In order to measure the absorption coefficient of the GST on top of the waveguides, we have used an architecture that compromises a microring-like (race track) resonator coupled to a nanophotonic waveguide (**Fig. 2a**). The fabrication process of these devices consists of the two main procedures described below.

Nanophotonic circuit fabrication

The fabrication of the waveguides and the microrings from silicon nitride-on-insulator substrates requires two e-beam lithography steps. First, alignment markers, which will be used for proper positioning of the subsequent e-beam expositions, are defined using a positive tone resist. After

developing the resist (in our case PMMA) a metal layer consisting of 5nm of Cr and 100nm of Au is evaporated on top of the sample. Subsequently, the PMMA is lifted off and the markers remain.

In a second exposure using the alignment markers for positioning, the pattern of the nanophotonic waveguides is written in ma-N 2403 negative tone resist and then developed. Later, dry reactive ion etching in CHF_3/O_2 chemistry is applied to etch down half of the Si_3N_4 thickness. Afterwards the exposed ma-N is removed to reveal the devices illustrated in **Fig.2a**.

The patterns of the nanophotonic circuits include two Bragg gratings separated by a distance of 250 μm (**Fig 2b**), used to couple light at a specific wavelength coming from a tunable laser source into the waveguides and to couple out the transmitted light at a second port [11]. Parameters like the gap between the waveguide and the race track, the width of the first and the radius of the latter were varied throughout the full chip.
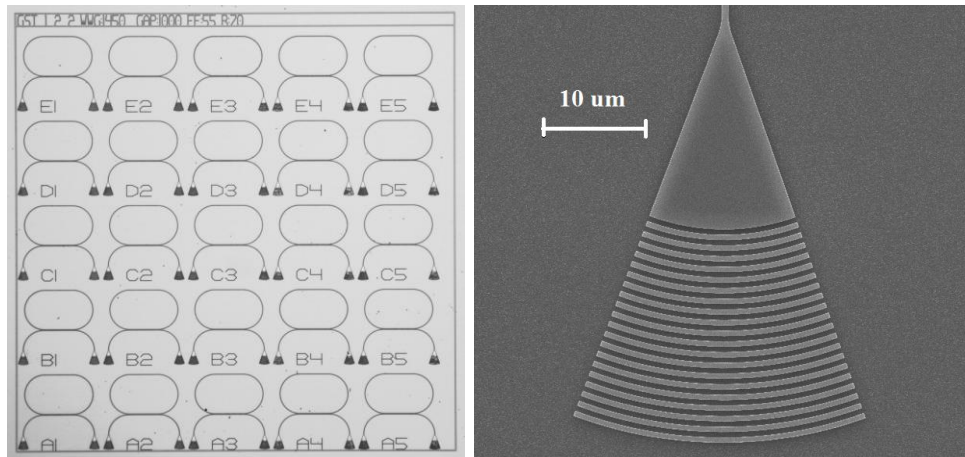

Fig. 2: *Left*: Optical micrograph of half-etched Si_3N_4 waveguides and microring resonators. The grating couplers were designed for five different wavelengths in the range 1.5-1.6μm and for five different (after) GST widths. *Right:* SEM image of a grating coupler designed for a wavelength of 1.52 μm

GST deposition

Once the nanophotonic circuits were fabricated, they are characterized optically in order to obtain the reference values for the resonances. When this is done, a further e-beam lithography step is required to write the masks where GST is going to be deposited. Using PMMA once again and the alignment markers as reference, rectangular patterns of 0.5, 1, 5, 10 and 20μm wide and 80 μm long are written on top of the free straight portions of the race tracks (**Fig. 3d**). After the development of the PMMA, 10nm of $Ge_2Sb_2Te_5$ was sputtered onto the sample followed by deposition of 10nm of ITO to avoid oxidation of the phase-change material.

With an average RMS surface roughness of 2.4 nm, AFM and SEM pictures of the GST layer for the five different widths are illustrated in **Fig. 3.** Only when the width is short, i.e., 0.5 or 1 μm, a curvature on top of the GST/ITO layer can be noticed as shown in **Fig. 3a**. The spikes on both sides are due to the lack of directionality in the sputtering process which results in the GST depositing on the PMMA sidewalls. The presence of the spikes was confirmed with SEM pictures as shown in **Fig. 3e.**
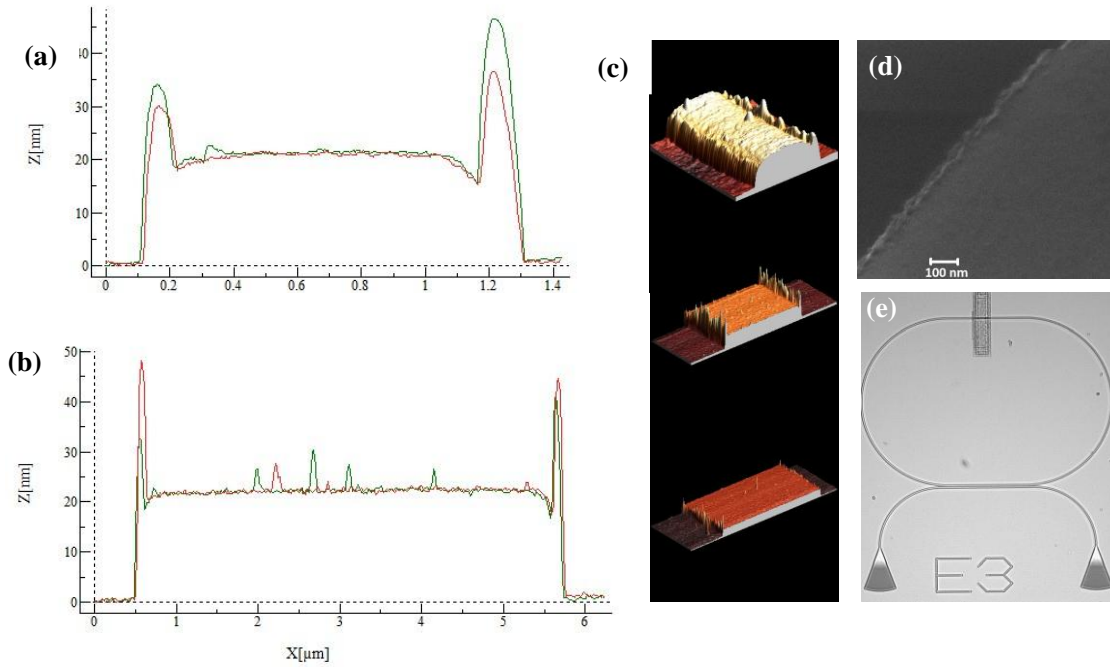
Fig. 3: AFM profile for the GST layers with width of (a) 0.5 µm and (b) 5 µm. (c) From top to bottom: 3D AFM images for GST widths of 0.5, 5, and 20µm. (d) SEM image: border of the 5 µm GST layer. (e) Device with GST on top at the end of all the fabrication process.

4. MEASUREMENTS AND RESULTS

Using a customized measurement setup including and optical fiber array, a telecom wavelength laser operating in the range 1.5-1.62µm and a power meter are connected to the nanophotonic circuit through the on-chip Bragg gratings. In the array the fibres are separated by 250µm, which corresponds to the separation of the two grating couplers within one device. The sample and the fibres are located on a computer controlled three-axis piezostage with sub 100nm alignment precision. Once the sample is placed on the stage, the position of the fibres is fixed to the point of highest transmission of the waveguides, measured with the powermeter.

Here we investigate four different kinds of devices with parameters given in **Table 1**. For each of the parameters, there were a total of five devices of type 1 and four of types 2, 3 and 4 each. The transmission and the average quality factor (Q) of these devices were measured before the GST deposition. Next, GST was deposited selectively on one part of the ring waveguides on all devices (shown in **Fig. 3e**) which remained in the amorphous state during all measurements. Different widths of: 0.5, 1, 5 and 10 µm; and also 20 µm in the case of the devices 1 were chosen for the GST strip. Subsequently, the transmission was measured once again.

Devices	Radius (µm)	Gap (µm)	Wavelength (µm)	Width (µm)	Q-factor
1	70	1.5	1,58	1.3	45000
2	100	1.0	1,58	1.3	10000
3	100	1.0	1,60	1.3	8000
4	100	1.3	1,58	1.3	25000

Table 1. Parameters for the four different devices used in the experimental measurements and the average Q-factor of the devices without GST. Width refers to the waveguide width.

A set of experimental measured peaks for the devices with and without GST at different widths are shown in **Fig. 4a**. We have determined the average wavelength shift for each resonance peak in the transmission spectrum with GST, with respect to the same device without GST. The results are presented in **Fig. 4b** where it can be seen that the set of devices 1 presents the highest shift as expected because in this case the radius is smaller and the gap bigger than for the other devices. A linear behaviour can be observed after 1 μm width for each set of devices (the device with 5 μm of GST in set 1 was damaged).

Then the Q-factor was measured for every single resonance peak using a Lorentz fit to the experimental data and then, with this information the absorption coefficient $\alpha_{dB}=10 \cdot \log_{10}e \cdot 2\pi n_g / \lambda Q$ was calculated [13]. The absorption coefficient of the GST was computed by substracting the absorption coefficient obtained from the resonance peaks with GST from the coefficient obtained without GST. In **Fig. 4c** is illustrated the dependence of α_{dB} with the wavelength in a small range were the maximum transmission for the waveguide is obtained. Next, an average over all the α_{dB} on one device was done for each GST width. The results are plotted in **Fig. 4d.** In spite of the different parameters used, the values for α_{dB} show a common general non-linear behaviour.
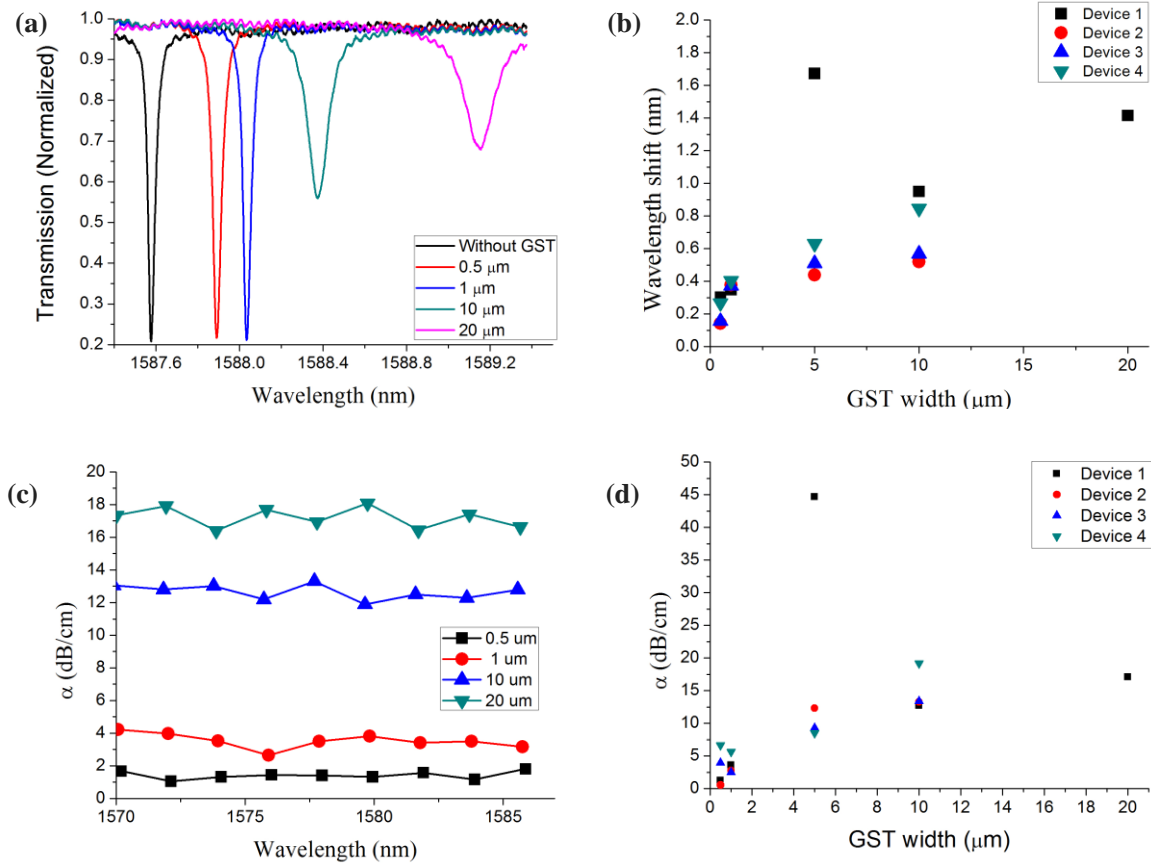
Fig. 4: (a) Transmission spectrum of devices 1 with their respective resonance peaks for different GST width. (b) Average of the wavelength shift due to the GST coverage for every device. (c) Absorption coefficient as a function of the wavelength for the devices 1 and (d) Absorption coefficient as a function of the GST width for every device.

4. CONCLUSION

The use of nanophotonic waveguides coupled to microring resonators allows for measuring the relevant optical properties of the GST, such as the absorption coefficient by following the evolution of the Q factor of the resonances. In particular, we have found that race tracks with the parameters described above for the devices 1 are the most suitable in order to obtain high Q-factors and therefore, easier and more accurate experimental measurements of the difference between resonators with and without GST in the amorphous state. New experiments involving more devices must be realized in order to obtain accurately the absorption coefficient as a function of the wavelength.

REFERENCES

1. J.Siegel, A.Schropp, J. Solis, C.N. Alfonso, and M. Wuttig, Appl. Phys. Lett **84** (2004) 2250.
2. D. Q. Huang, X. S. Miao, Z. Li, J. J. Sheng, J. J. Sun, J.H. Peng, J. H. Wang, Y. Chen and X. M. Long, Appl. Phys. Lett. **98** (2011) 242106
3. W. J. Wang, L. P. Shi, R. Zhao, K. G. Lim, H. K. Lee, T. C. Chong, and Y. H. Wu, Appl. Phys. Lett. **93** (2008) 043121.
4. M. Wuttig and N. Yamada, Nature Mater. **6** (2007) 824.
5. S. –H. Lee, Y. Jung and R. Agarwal, Nat. Nanotechnol. **2** (2007) 626.
6. S. Raoux et al., IBM J. Res. Dev. **52** (2008) 465.
7. H. P. Wong et al. Proc. IEEE **98** (2010) 2201.
8. S. Kim et al., IEEE Trans. Electron Devices **58** (2011) 1483.
9. S. Y. Kim, S. J. Kim, H. Seo, and M. R. Kim, Proc. SPIE **3401** (1998) 112.
10. W. H. P. Pernice, and H. Bhaskaran, App. Phys. Lett. **101** (2012) 171101.
11. K. Fong, W. Pernice, M. Li, and H. Tang, Appl. Phys. Lett. **97** (2010) 073112.
12. A. Gondarenko, J. A. Levy, and M. Lipson, Opt. Express **17** (2009) 11366.
13. P. Rabiei, W. H. Steier, C. Zhang, and L. R. Dalton, J. Lightwave Technol. **20** (2002) 1968.